Final Report on the

ADVANCEMENT IN THE STATE OF THE ART IN THE PRODUCTION OF FIELD SOLAR CELLS

Prepared for
NASA/Goddard Space Flight Center
Glenn Dale Road
Greenbelt, Maryland 20771
Attention: Contracting Officer, Code 247

Contract NAS5-9612

EOS Report 6973-Final 16 December 1965

Prepared by
P. Rolik, Project Supervisor

Approved by
S. Kaye, Manager
Solid State Laboratory

Approved by

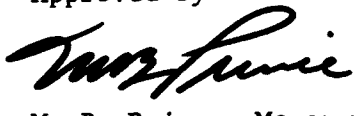

M. B. Prince, Manager
PHYSICAL INSTRUMENTATION GROUP

ELECTRO-OPTICAL SYSTEMS, INC. — PASADENA, CALIFORNIA
A Subsidiary of Xerox Corporation

ADVANCEMENT IN THE STATE OF THE ART IN THE PRODUCTION OF FIELD SOLAR CELLS

Staff, Physical Instrumentation Group

Electro-Optical Systems, Inc.
A Subsidiary of Xerox Corporation

29520

ABSTRACT

The results of a further study to develop an improved radiation-resistant solar cell by the incorporation of an electrical field are described. Included are the results of a theoretical computer evaluation, drift field fabrication experiments, and radiation damage data.

The radiation damage data shows the results of saturation current and the diode equation A factor change as a result of irradiation on a sample group of cells. The degradation characteristics of these cells are also given under tungsten and sunlight illumination.

CONTENTS

ILLUSTRATIONS

1. INTRODUCTION

The technical objectives of this contract were threefold. One objective was to extend the previous efforts conducted in theoretical studies on drift field solar cells (Refs. 1 and 2). Another was to examine the possibilities of changing the drift field configurations in order to further decrease the rate of degradation of short-circuit current of solar cells when exposed to energetic particle bombardment. In addition, the problem of open-circuit voltage degradation was investigated since this parameter is important in determining the end-of-life output power obtainable from such cells. Solar cells fabricated in accordance with these theories were submitted to the technical monitor for radiation-damage testing.

Several parameters contributing to open-circuit voltage degradation were investigated on a group of cells prior to and after irradiation. These included saturation currents, "A" factors and current versus voltage characteristics in sunlight and tungsten illumination.

Cells of three types were fabricated from 1, 10, and 25 ohm-cm starting silicon material. The basic process employed a diffused drift field in the base material and a low-resistivity, epitaxial layer on the back side of the cell adding to its thickness and strength. Sintered, silver-titanium contacts and silicon monoxide, antireflection coatings were employed.

2. THEORY OF DRIFT FIELD CONFIGURATION

The data necessary to program the computer for numerical solution of the diode continuity equation was submitted to the technical monitor. This present solution takes into account a high drift field toward the back of the cell, whereas previous work on a solution considered a high drift field toward the front of the cell (Ref. 2). This required a change in the boundary conditions necessary for evaluation of the various constants in the solution. The data and the conditions necessary for programming are given in the appendix of this report. (The results are shown in Fig. 1.)

In comparing this to the results obtained by EOS under NASA Contract NAS5-3560 (Ref. 1) which assumed a high field toward the front of the cell (Fig. 2), it would be reasonable to assume that a more efficient cell results by utilizing a high field strength near the junction, although this was not intuitively obvious. The two types of field profiles considered for the calculations of current collection efficiency are shown in Fig. 3. Case I assumes a linear change of field strength through the active base region, with the highest field at the p-n junction. Case II again assumes a linearly changing field, but with the high field at the back of the active region. It should be noted here that if the field is formed by a long diffusion of an acceptor-type dopant into p-type base material from the back, the impurity distribution being an erfc, a field profile approaching Case I is attained. Also, the average field strength (assuming a 10^5 ratio in the number of impurities) is approximately $0.3/w$ volts cm^{-1}, where w is the field width. This would give a field varying linearly from zero to $0.6/w$ volts cm^{-1}. Also, for the purpose of approximation, both μ and τ were assumed to decrease linearly with position as one proceeds toward the heavily doped portions of the base

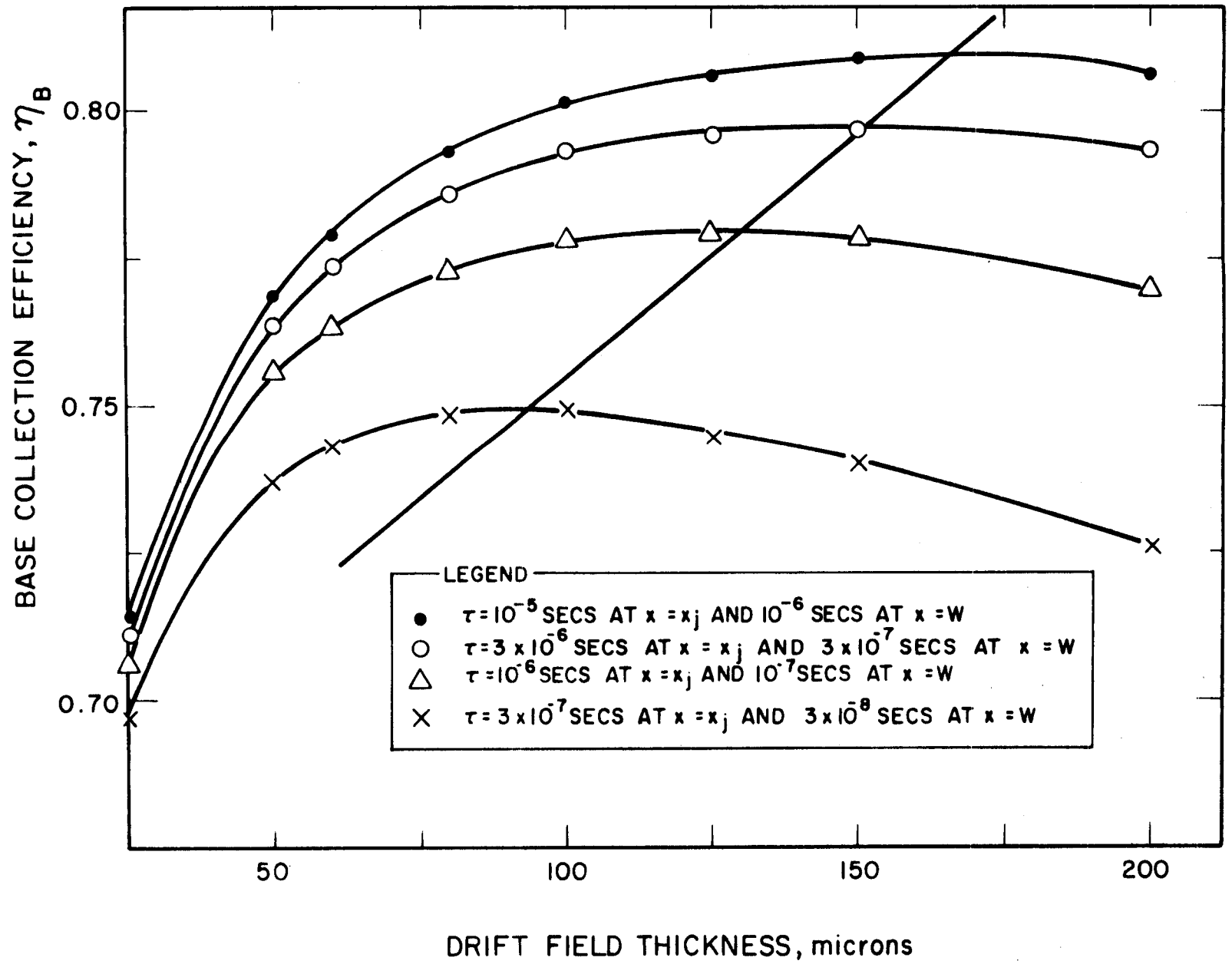

FIG. 1 RESULTS OF COMPUTER SOLUTION FOR DRIFT FIELD CELL WITH HIGH FIELD NEAR THE JUNCTION

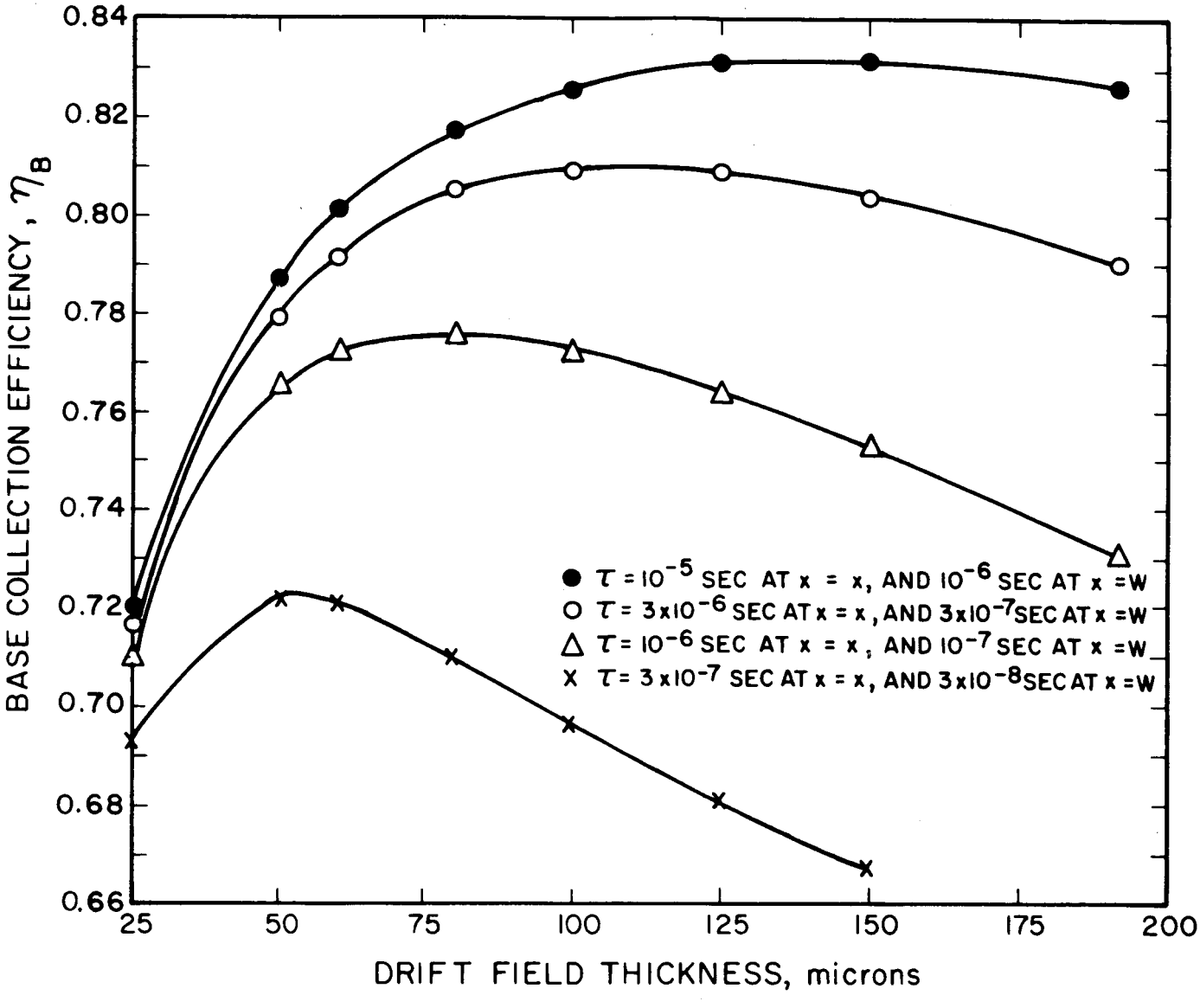

FIG. 2 RESULTS OF COMPUTER SOLUTION FOR DRIFT FIELD CELL WITH HIGH FIELD AT THE BACK

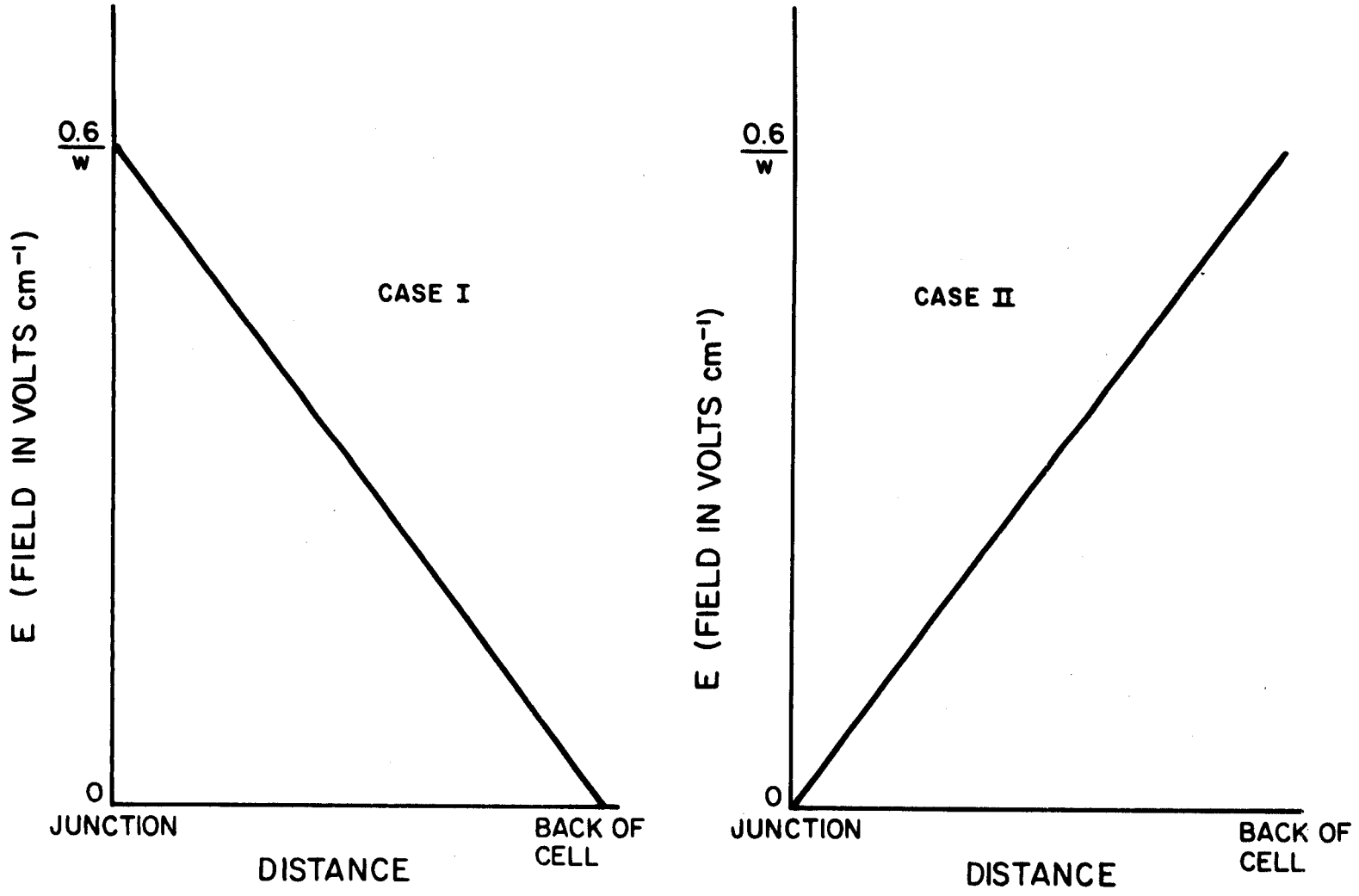

FIG. 3 FIELD DISTRIBUTION VERSUS DEPTH IN DRIFT CELL

region. These assumptions also can be justified by considering both μ and τ to be valued low in the low resistivity material at the back of the cell and increasing to higher values in the high resistivity material at the front of the cell (Ref. 2). In comparing the results of the calculation as shown in Figs. 1 and 2, no vast difference is seen between the two cases, although a smaller optimum field width and lower base collection efficiency is predicted for Case II. The sample cells fabricated during the course of the contract were designed in light of this investigation.

3. CELL FABRICATION

3.1 Drift Field Diffusion

Solar cell blanks, 1 x 2 cm, p-type, and of 1, 10, and 25 ohm-cm resistivity were initiated through the process of drift field fabrication. This was performed by depositing boron with a surface concentration of approximately 7×10^{19} atoms/cm^3 on one polish-etched side of the blanks and diffusing them at a temperature of 1300°C for a period of 64 hours. Assuming a complementary error function distribution, a field depth of approximately 80 microns should have resulted. This was verified by evaluating 1 ohm-cm n-type control slices, processed along with the p-type blanks, by angle sectioning and stain etching, which resulted in a junction depth of approximately 90 microns, confirming the theoretical calculations to an error of within 10 percent.

3.2 Drift Field Evaluation

Several samples of the p-type diffused blanks were evaluated by successive etching and 4-point-probe measurements. The resulting impurity concentration profile versus the theoretical curve is shown in Fig. 4. The theoretical value of surface concentration, 1.2×10^{19} atoms/cm^3, was obtained by the measurement of sheet resistance and junction depth on the control slices (Ref. 3). It should be noted that the surface concentration had dropped from the initial figure of 7×10^{19} to the lower figure during the long diffusion period. It should also be noted that this lower value of surface concentration was verified by the successive etch-and-probe technique. However, the anomalous result obtained in the 60- to 90-micron region of the diffused field cannot be adequately explained. It is possible that because of the close proximity of the back of the slice to the probe, as the sample became thinner, inaccuracies in probe measurement were obtained. No probe correction factor was applied.

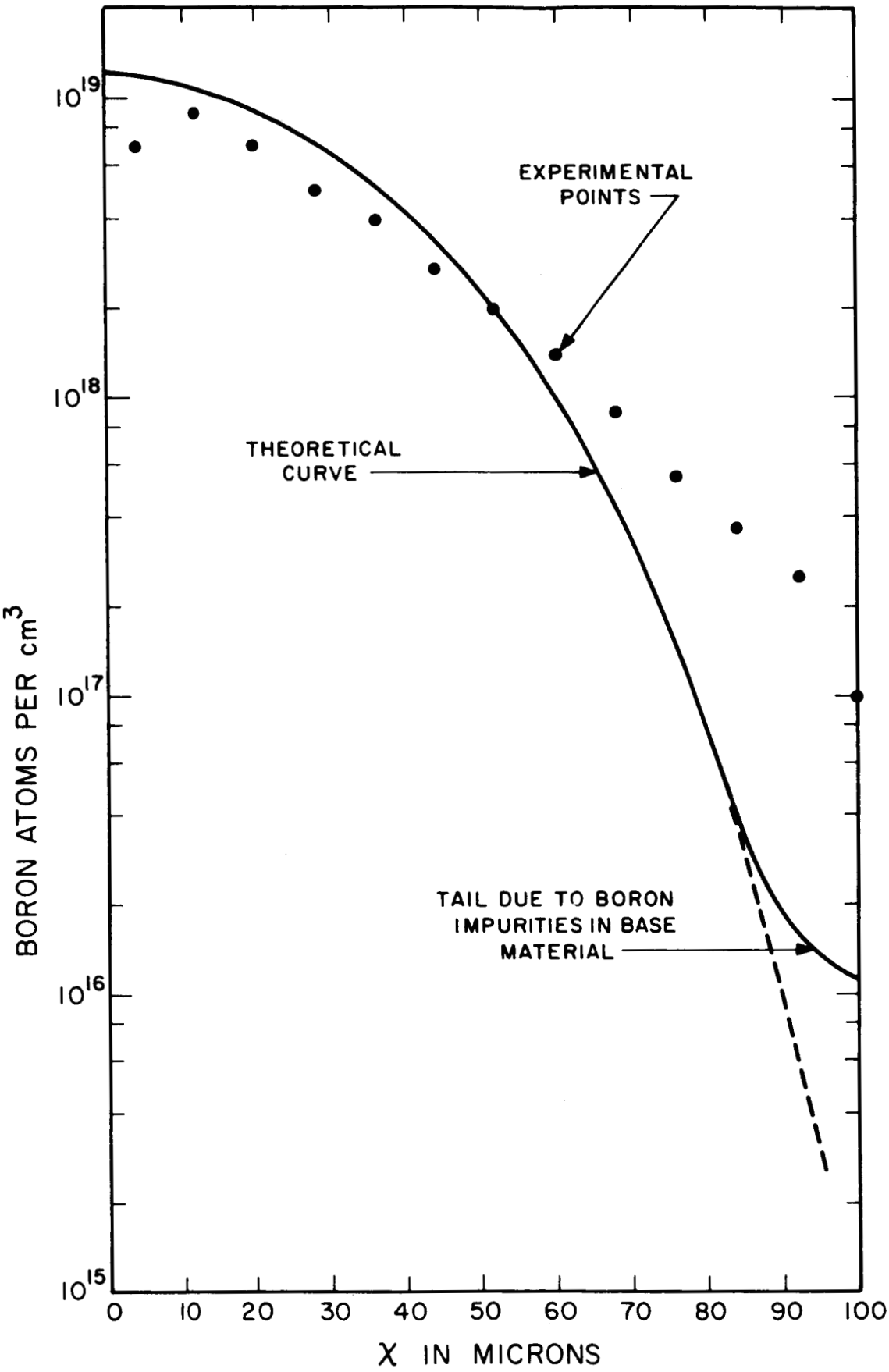

FIG. 4 BORON CONCENTRATION DISTRIBUTION VERSUS DISTANCE IN 1 OHM-CM CELLS

3.3 Epitaxial Growths

The passive region at the back of the cell was grown by conventional epitaxial techniques using the hydrogen reduction of silicon tetrachloride. (Figure 5 shows a schematic diagram of the growth apparatus.) The growths were of low resistivity (approximately 0.005 ohm-cm), and the doping performed by addition of boron tribromide to the silicon tetrachloride in the bubbling bottle. The first growths attempted were not of good, single crystalline quality, and yielded cells with poor electrical characteristics. Dislocation etches performed on the n-type surfaces of the cells fabricated from these first growths displayed dislocation pits, singly, in clusters, and in long lines of the top surfaces. These imperfections are thought to be because of plastic deformation of the single crystalline layers. This was attributed to thermal coefficient of expansion differences between these and the imperfect growths. Later runs yielded much better cells and dislocation etching did not display large numbers of etch pits.

3.4 Junction Diffusion

After lapping and polish etching of the p-type diffused samples to the edge of the field region, an n-type layer was formed on the top surface by phosphorous diffusion forming the p-n junction. This diffusion was performed at a temperature of 930°C for a period of 30 minutes, yielding an 0.3- to 0.4-micron deep p-n junction in the 1 ohm-cm substrate. The junction depth was verified by conventional angle sectioning and stain etching techniques.

3.5 Contact Application and Antireflection Coating

After removal of the oxide layer formed by the phosphorous diffusion, grid-type contacts of sintered silver-titanium were applied to the cells. Approximately 200 to 300Å of titanium and 15 to 20 microns of silver was evaporated onto the samples through a suitable grid mask. The sintering was performed at a temperature of 730°C for a period of 3 minutes. After suitable masking, the edges of the cells

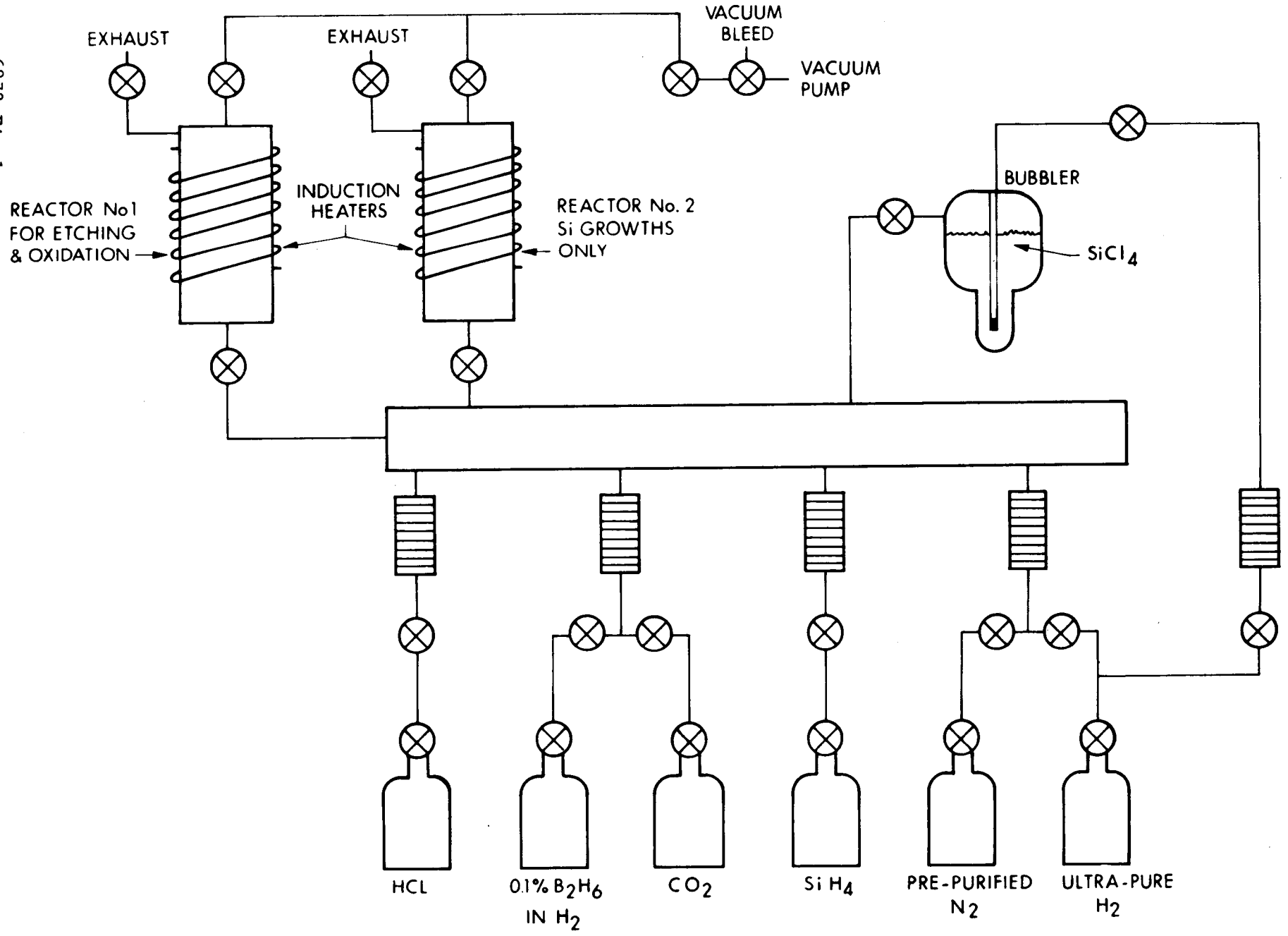

FIG. 5 SCHEMATIC DIAGRAM OF SILICON EPITAXIAL SYSTEM

were etched in a hydrofluoric-nitric acid solution to remove the evaporated metal and to clean the junction periphery. Antireflection coatings were applied by vacuum evaporation of silicon monoxide. The coating thickness was optimized for sunlight illumination.

4. CELL EVALUATION

Spectral responses were taken on a few selected cells of the 1 ohm-cm type, employing a modified Perkin-Elmer Model 13 monochromator. The data were plotted on both a constant energy and a constant-photon basis, with the peak in the constant-energy case occurring at approximately 7000Å. This indicated that 1 ohm-cm material possessed too low a lifetime for consideration as drift field cell material. Spectral response measurements taken on representative samples of 10 ohm-cm cells indicated the peak response to occur at approximately 7500Å to 8000Å.

I-V characteristics taken under tungsten illumination showed the 1 ohm-cm cells to have conversion efficiencies between 5 to 7 percent and the 10 and 25 ohm-cm cells to have conversion efficiencies in the 6 to 8 percent range. The results are shown in Tables Ia to Ic. The tungsten light was calibrated with an n on p standard cell, and consequently the efficiencies are low. However, in sunlight illumination, the efficiencies increased by 15 to 23 percent. (See Table II.) The reason for this is that the peak response of the drift field cells occurs at about 7500 to 8000Å if considered on a constant energy basis.

In order to investigate the open-circuit voltage degradation question, the saturation currents on several sample cells were determined. This was done by measuring the slope of current versus voltage in the 0 to +5 millivolt region, with the cell in complete darkness. The shunt resistance of the cell was determined by considering the slope of the voltage versus current in the 0.5 to 1.5V region. The procedure for determination of I_o can be explained by considering the following equations:

TABLE Ia

TUNGSTEN EFFICIENCIES AND SHORT-CIRCUIT CURRENT OF CELLS FABRICATED FROM 1 OHM-CM MATERIAL

Cell No.	Efficiency in Percent	I_{sc} in amps x 10^{-3}	Cell No.	Efficiency in Percent	I_{sc} in amps x 10^{-3}
E54-5a	5.2	29.5	E54-8a	6.8	30.0
E54-6a	5.5	26.0	E54-8b	6.4	29.0
E54-7b	6.4	30.0	E54-8c	5.7	27.0
E54-7c	6.3	28.5	E54-9a	6.4	29.0
E54-7d	6.5	30.0	E54-9b	5.9	28.5

TABLE Ib

TUNGSTEN EFFICIENCIES AND SHORT-CIRCUIT CURRENT OF CELLS FABRICATED FROM 10 OHM-CM MATERIAL

Cell No.	Efficiency in Percent	I_{sc} in amps x 10^{-3}	Cell No.	Efficiency in Percent	I_{sc} in amps x 10^{-3}
E55-1a	6.9	32.0	E56-2c	7.1	32.5
E55-1b	8.2	37.5	E56-2f	7.0	33.5
E55-1c	6.8	32.5	E56-3d	6.6	31.5
E55-2a	6.7	28.5	E56-4a	7.8	34.5
E55-2b	6.5	29.0	E56-4c	7.0	31.5
E55-2c	6.7	29.0	E56-3a	6.8	31.0
E55-2d	7.0	31.0	E56-1c	6.9	31.5
E55-3a	6.1	26.5	E57-1	6.7	35.5
E55-3b	6.9	29.5	E57-2	6.9	33.0
E55-4b	6.4	26.5	E57-3	6.4	30.0
E56-1a	8.1	37.0	E57-4	6.5	29.5
E56-1d	6.7	32.0	E57-5	7.7	36.5
E56-1f	6.5	30.0	E57-6	7.0	36.0
E56-2a	7.0	30.5	E57-7	7.5	34.5
E56-2b	7.4	33.5	E57-9	6.1	31.0
E56-2c	7.5	31.5	E57-10	7.1	35.0

TABLE Ic

TUNGSTEN EFFICIENCIES AND SHORT-CIRCUIT CURRENT
OF CELLS FABRICATED FROM 25 OHM-CM MATERIAL

Cell No.	Efficiency in Percent	I_{sc} in amps x 10^{-3}	Cell No.	Efficiency in Percent	I_{sc} in amps x 10^{-3}
E58-1	7.6	36.0	E58-16	5.5	28.5
E58-2	7.6	39.5	E58-17	7.9	38.5
E58-3	8.2	41.5	E59-1	7.2	37.0
E58-4	7.5	35.5	E59-3	6.3	31.0
E58-5	7.8	39.0	E59-5	6.4	34.5
E58-6	6.9	30.0	E59-6	6.7	33.5
E58-7	7.8	37.5	E59-7	5.9	32.0
E58-8	5.5	29.0	E59-8	7.7	36.5
E58-9	7.4	39.0	E59-9	7.4	34.0
E58-10	6.1	35.0	E59-10	7.0	35.5
E58-11	5.7	30.5	E59-11	6.4	35.0
E58-12	6.5	35.5	E59-12	6.8	34.5
E58-13	7.4	39.0	E59-135	7.5	38.0
E58-14	7.0	36.0	E59-155	6.6	38.0
E58-15	7.4	39.5			

TABLE II

I_o, SHORT-CIRCUIT CURRENT AND EFFICIENCY IN TUNGSTEN AND SUNLIGHT BEFORE IRRADIATION

Cell No.	Tungsten I_{sc} in Amps	Tungsten Efficiency in Percent	Sunlight I_{sc} in Amps	Sunlight Efficiency in Percent	Sunlight over Tungsten Efficiency Increase in Percent
56-1a	37.0×10^{-3}	8.1	43.0×10^{-3}	9.4	16
56-1c	31.5×10^{-3}	6.9	38.0×10^{-3}	8.2	18
56-1d	32.0×10^{-3}	6.8	39.0×10^{-3}	8.2	20
56-1f	30.0×10^{-3}	6.5	37.0×10^{-3}	8.0	23
56-2a	30.5×10^{-3}	7.0	37.0×10^{-3}	8.5	21
56-2b	33.5×10^{-3}	7.4	39.0×10^{-3}	8.6	16
56-2c	32.0×10^{-3}	7.5	38.5×10^{-3}	8.9	18
56-2d	32.5×10^{-3}	7.1	38.5×10^{-3}	8.4	18
56-2f	33.5×10^{-3}	7.0	39.5×10^{-3}	8.2	17
56-3a	31.0×10^{-3}	6.8	37.0×10^{-3}	8.0	17
56-3d	31.5×10^{-3}	6.6	37.0×10^{-3}	7.8	18
56-4a	34.5×10^{-3}	7.8	39.5×10^{-3}	8.9	14
56-4c	31.5×10^{-3}	7.0	37.0×10^{-3}	8.2	17

$$I = I_o \exp\left(\frac{qV}{KT}\right) - I_o + \frac{V}{R_{SH}} \quad (1)$$

$$\frac{dI}{dV} = I_o \frac{q}{KT} \exp\left(\frac{qV}{KT}\right) + \frac{1}{R_{SH}} \quad (2)$$

$$I_o = \frac{KT}{q}\left[\frac{dI}{dV} - \frac{1}{R_{SH}}\right] \text{ as } V \rightarrow 0 \quad (3)$$

where

I_o = saturation current
V = output voltage
R_{SH} = shunt resistance
q = electronic charge
K = Boltzmann's constant
T = temperature in ^oK

The A factor was not taken into account in these calculations since even small deviations from A = 1 would affect only small discrepancies in the calculation of I_o. The values of I_o obtained before and after irradiation with 10^{16} 1μ eV electrons cm^{-2} are listed in Table III.

However, in evaluating the total power available from the cell at the maximum power point, the A factor becomes important in determining the current flowing internally in the cell. This can be shown by considering the diode equation:

$$I = \left[I_o \exp\left(\frac{qV}{AKT}\right) - I_o + \frac{V}{R_{SH}}\right] - I_L \quad (4)$$

The bracketed term represents that portion of the current dissipated internally subtracting from the light generated current I_L. As the A factor decreases in the exponential term, the total I_L delivered to the outside circuit of the cell becomes less and the power of the cell deteriorates, this being in addition to the loss of I_L due to a decrease of collection efficiency.

TABLE III

I_o OF 10 OHM-CM CELLS BEFORE AND AFTER IRRADIATION

Cell No.	I_o Before Irradiation in Amps	I_o After Irradiation in Amps
E56-1a	1.15×10^{-7}	1.6×10^{-7}
E56-1d	1.81×10^{-6}	8.2×10^{-7}
E56-1f	3.68×10^{-8}	3.1×10^{-8}
E56-2a	2.8×10^{-8}	1.0×10^{-7}
E56-2b	4.3×10^{-8}	4.7×10^{-7}
E56-2c	5.2×10^{-8}	1.3×10^{-7}
E56-2d	3.9×10^{-8}	3.3×10^{-8}
E56-4a	5.6×10^{-8}	7.5×10^{-8}
E56-4c	3.9×10^{-8}	6.0×10^{-8}

Consequently, A factors were determined before and after irradiation on the same group of cells on which I_o measurements had been taken. The calculations were made by measuring the short circuit current I_{SC} and open circuit voltage V_{OC} at various light intensities and substituting in the relation:

$$A = \frac{q}{KT} \frac{V_{OC}}{\ln\left[\frac{I_{SC}}{I_o} + 1\right]} \qquad (5)$$

the value of I_o used, being that which had been determined experimentally as mentioned above. The data is shown in Figs. 6 through 14. The general decrease of the A factor after irradiation on all the cells tested indicates that irradiation causes a deterioration not only by the decrease of short circuit current, but also by an increase of the internally dissipated current.

Tables IV and V show results of cell characteristics under tungsten and sunlight illumination before and after irradiation.

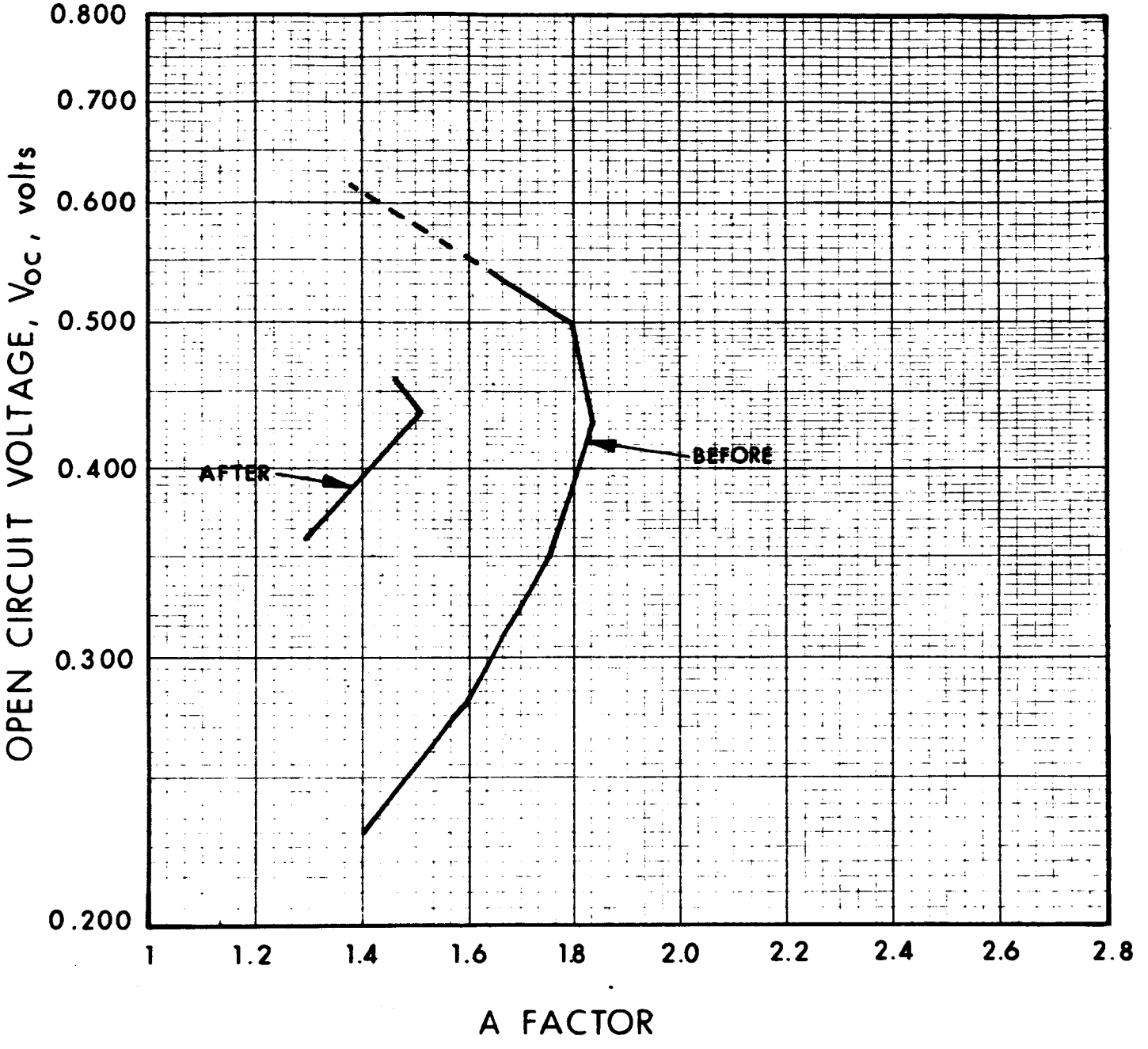

FIG. 6 CELL E56-1a

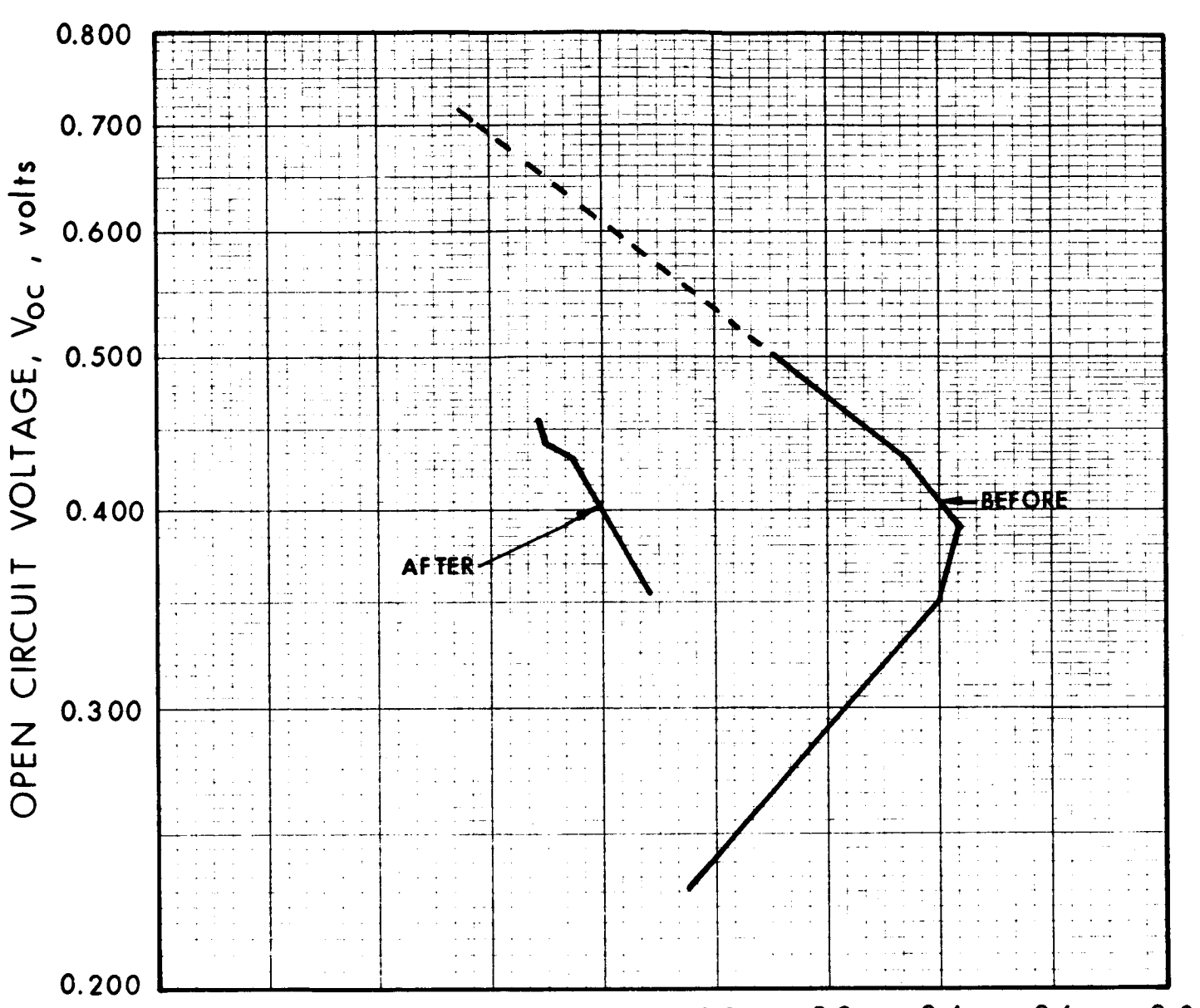

FIG. 7 CELL E56-1d

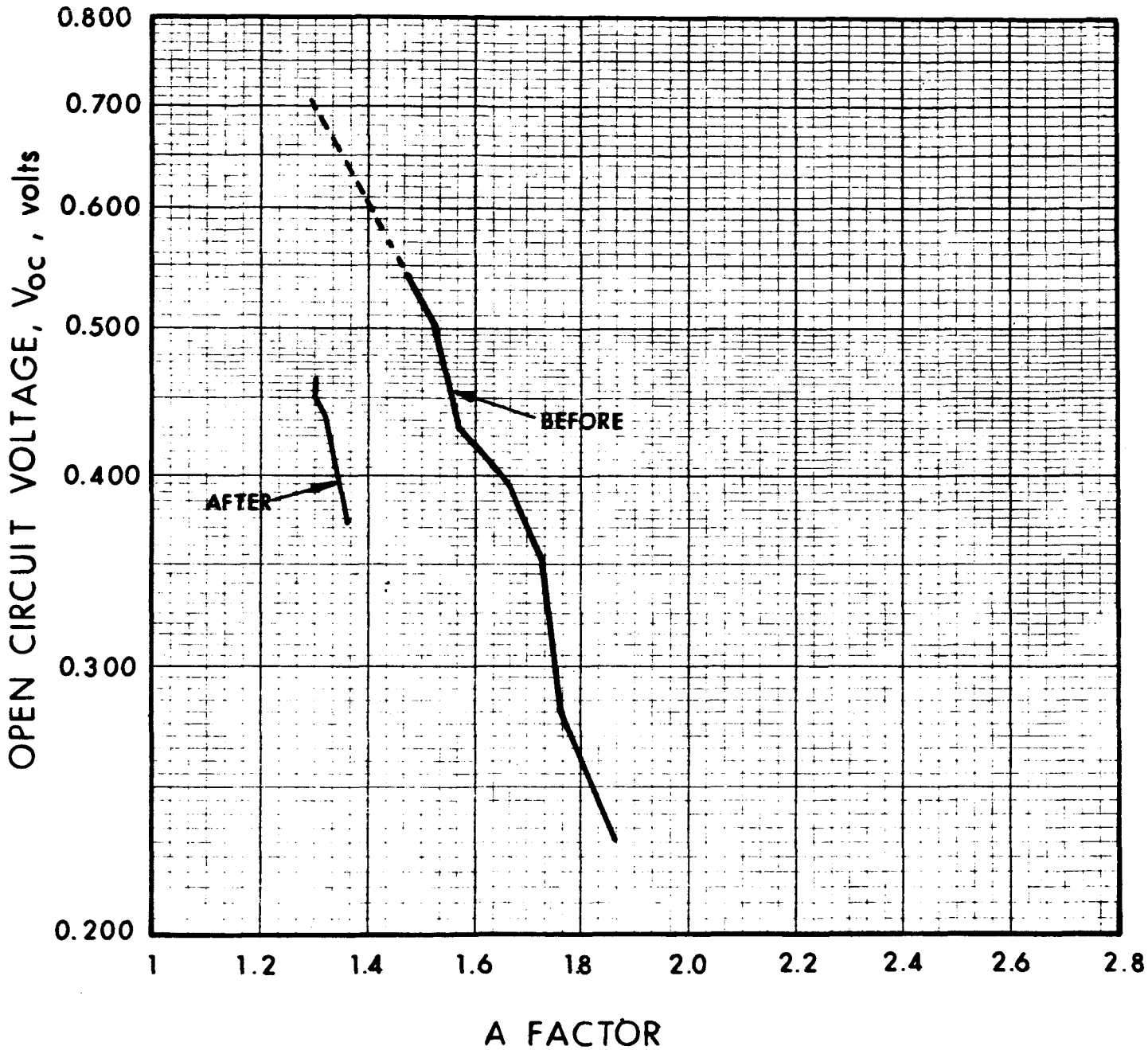

FIG. 8 CELL E56-1f

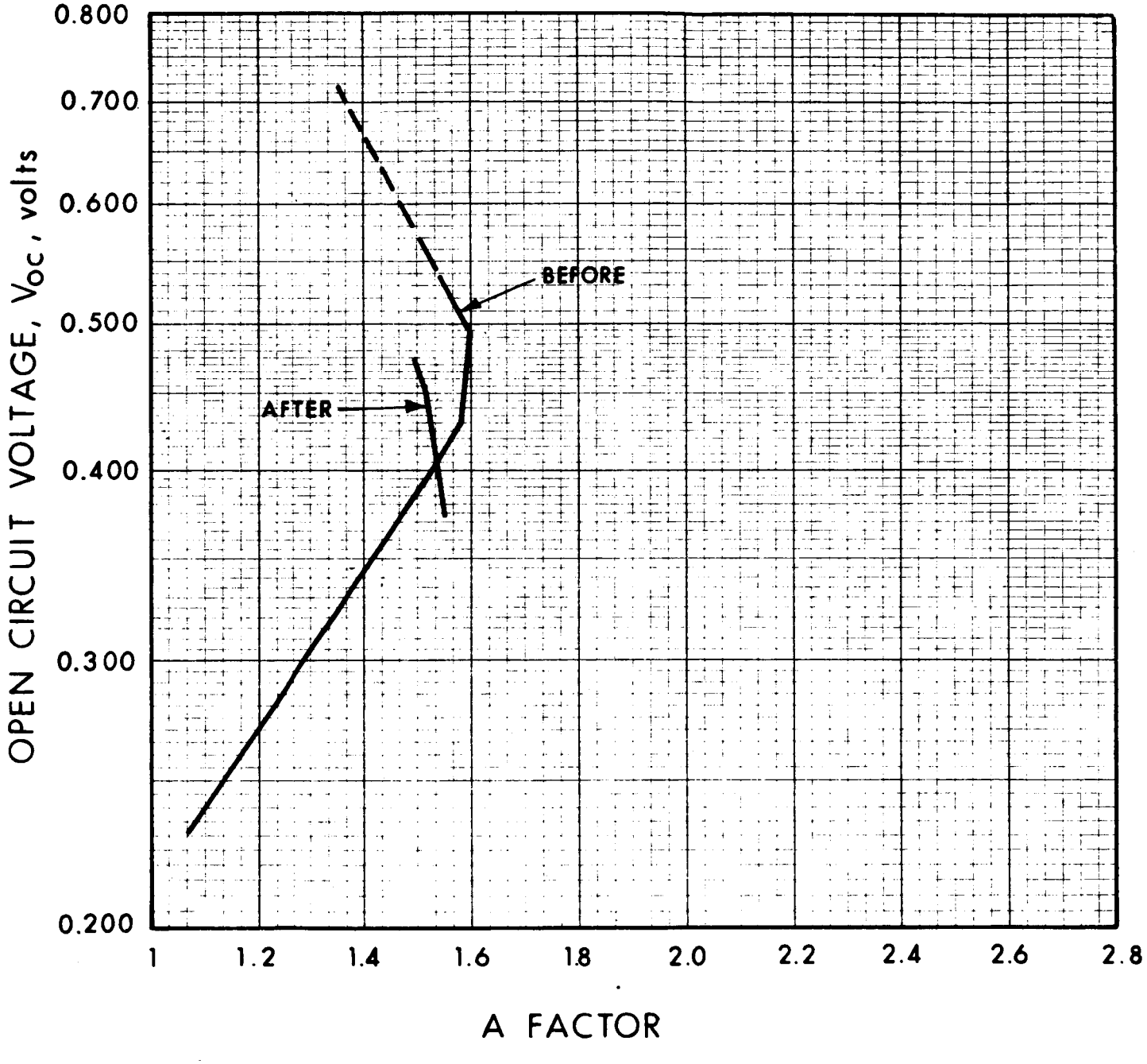

FIG. 9 CELL E56-2a

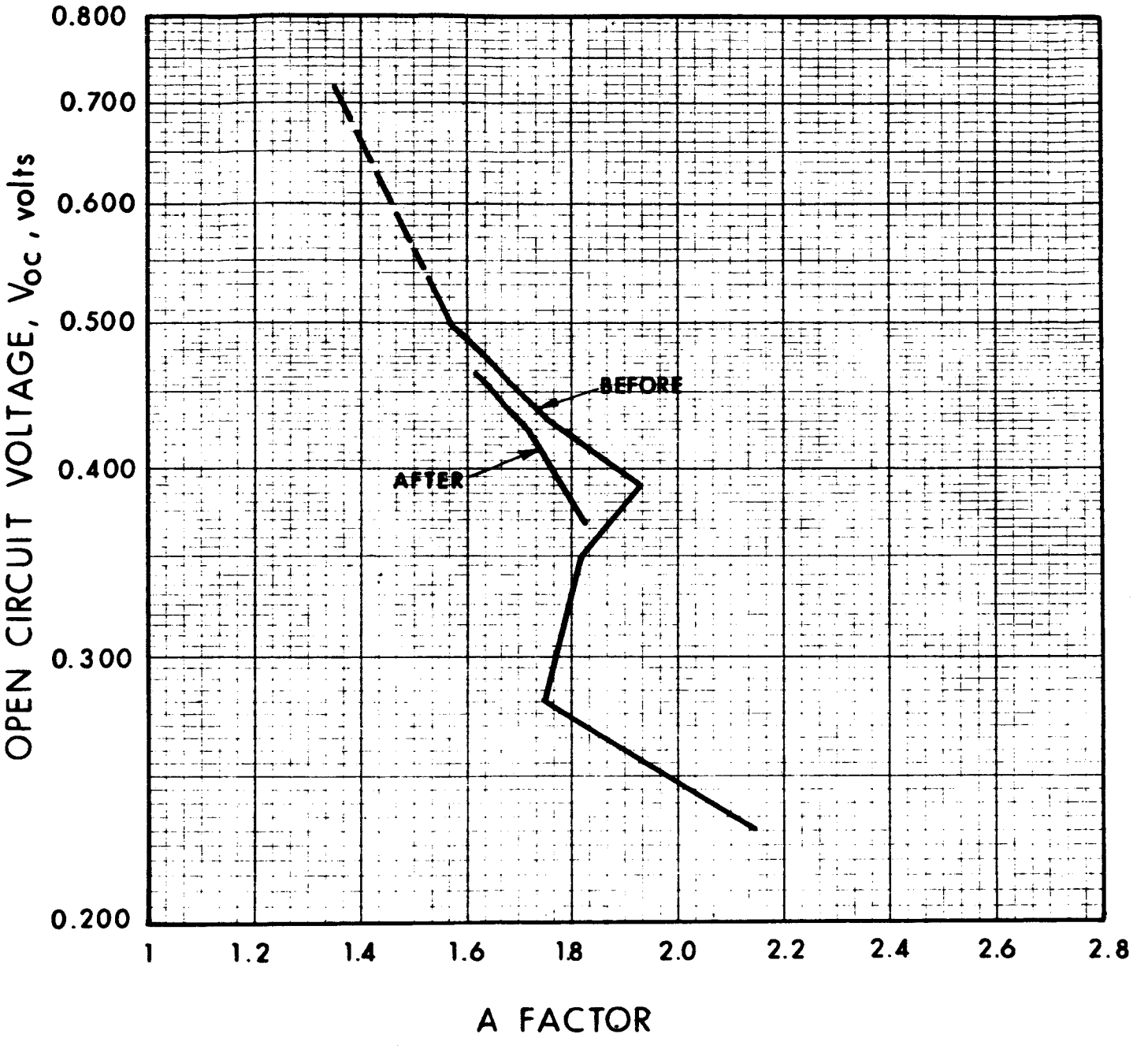

FIG. 10 CELL E56-2b

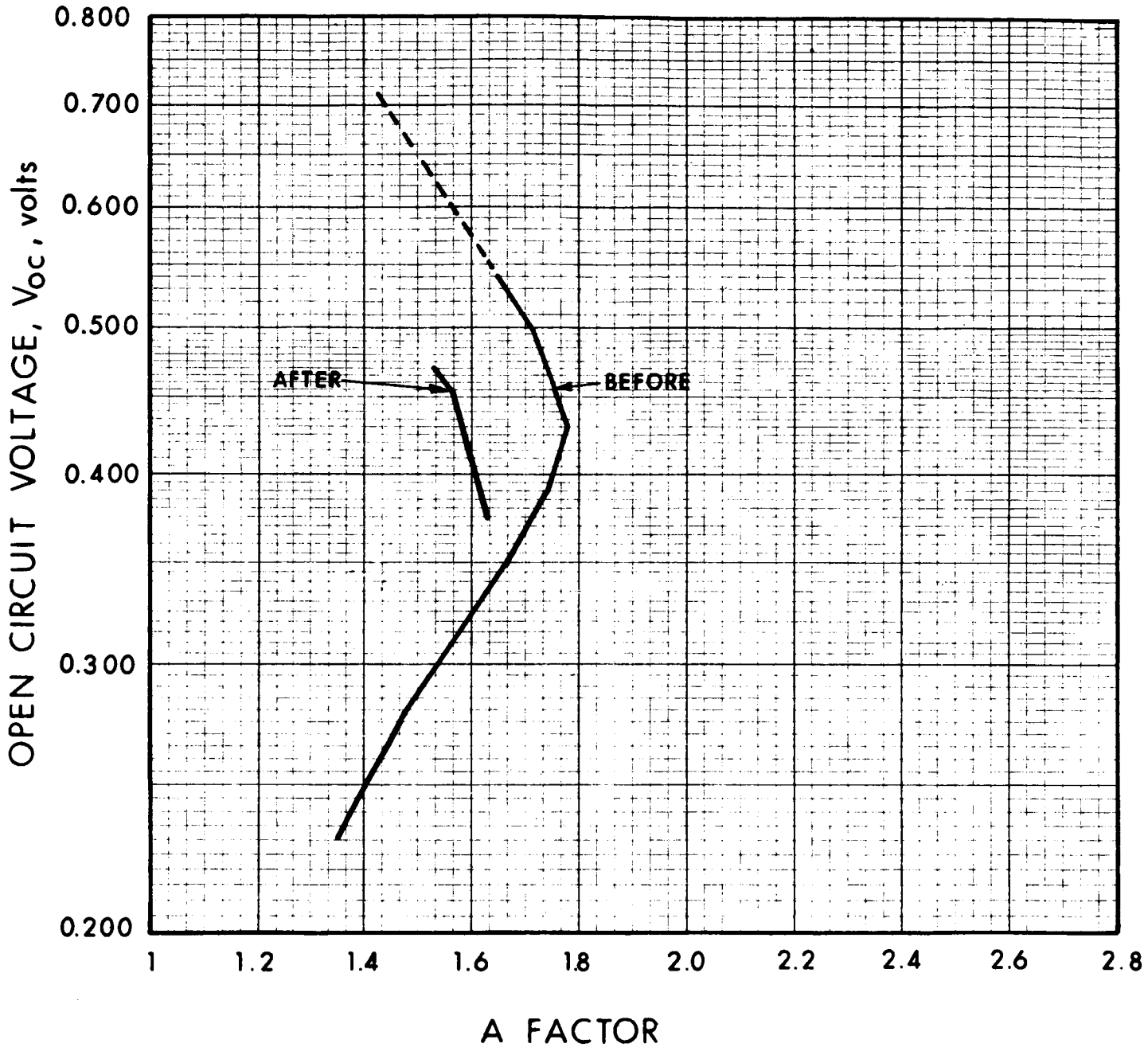

FIG. 11 CELL E56-2c

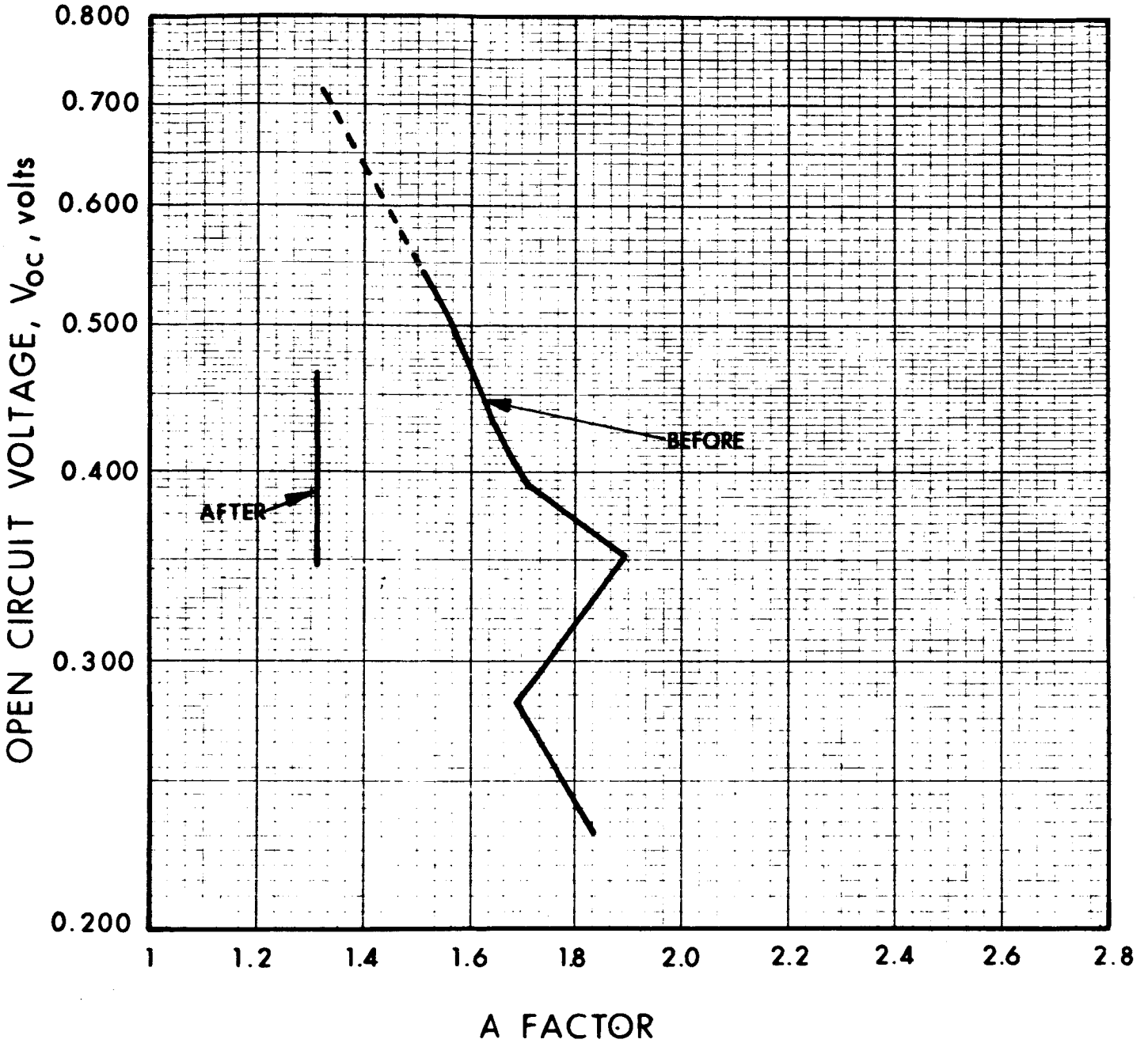

FIG. 12 CELL E56-2d

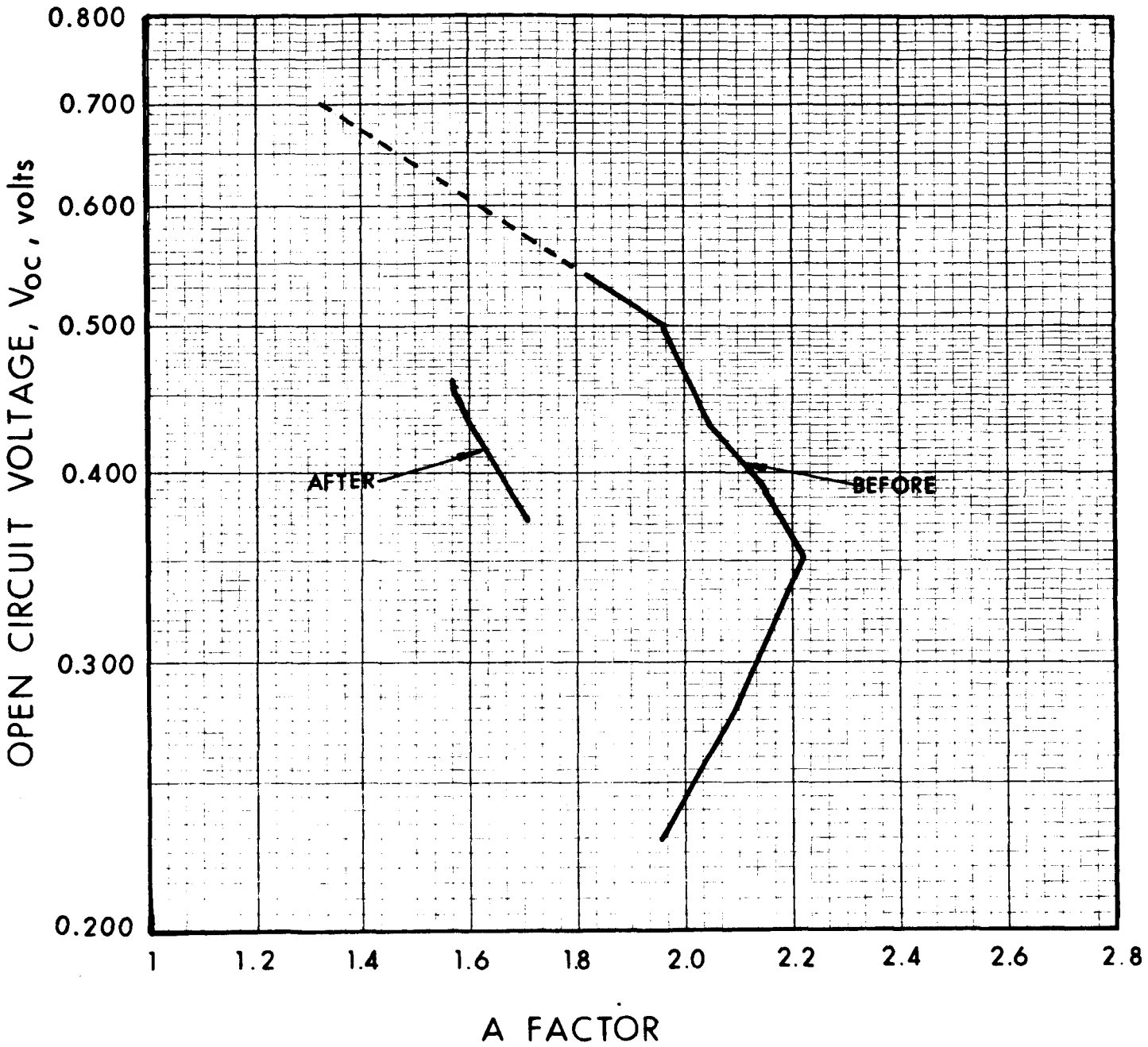

FIG. 13 CELL E56-4a

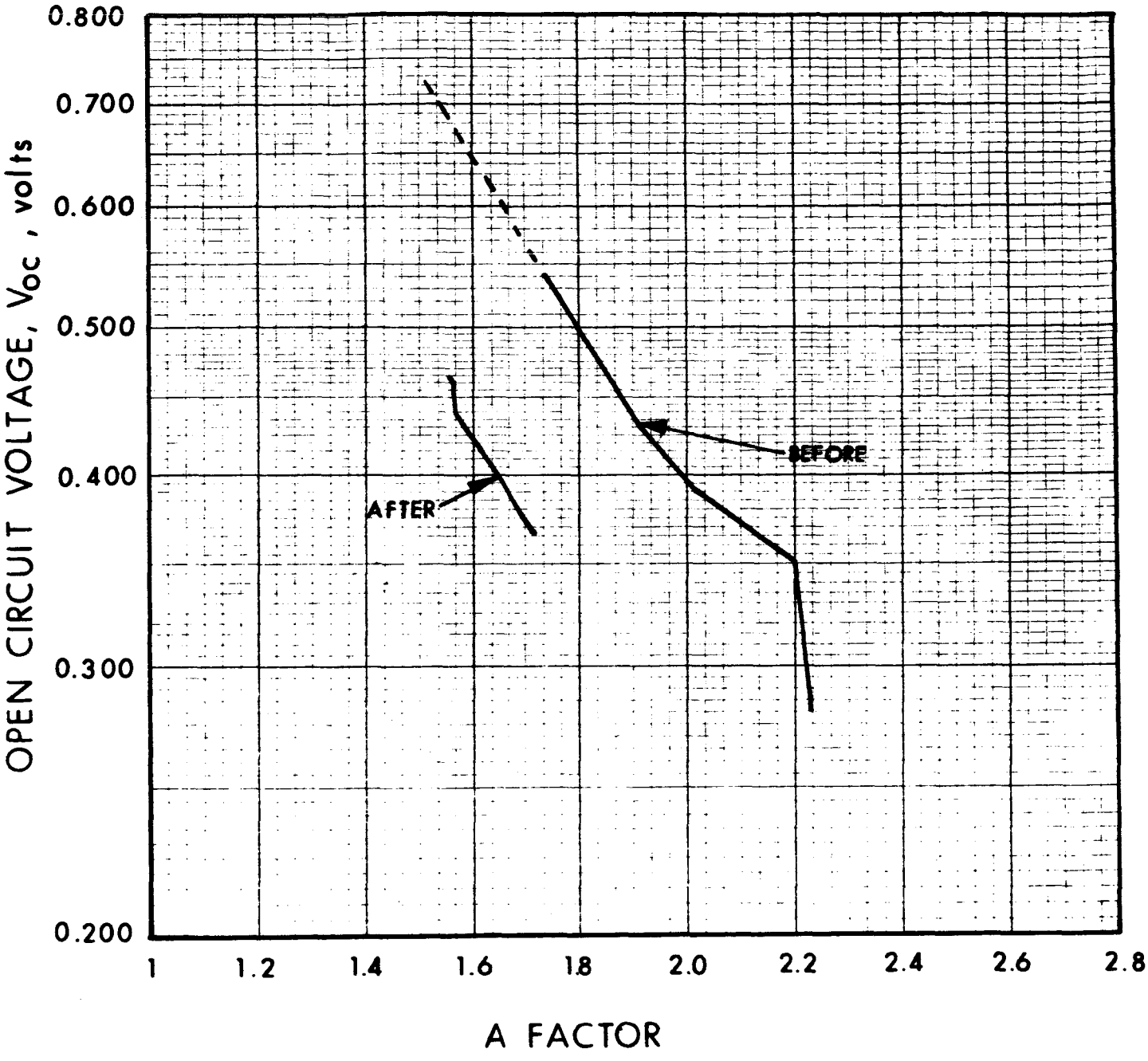

FIG. 14 CELL E56-4c

TABLE IV

SHORT-CIRCUIT CURRENT AND EFFICIENCY IN TUNGSTEN AND SUNLIGHT AFTER IRRADIATION

Cell No.	Tungsten I_{sc} in Amps	Tungsten Efficiency in Percent	Sunlight I_{sc} in Amps	Sunlight Efficiency in Percent	Sunlight Over Tungsten Efficiency Increase in Percent
56-1a	23.7×10^{-3}	4.4	32.6×10^{-3}	6.2	14
56-1d	23.0×10^{-3}	4.0	32.0×10^{-3}	5.6	14
56-1f	20.5×10^{-3}	3.8	28.7×10^{-3}	5.3	14
56-2a	16.5×10^{-3}	3.0	24.7×10^{-3}	4.5	15
56-2b	21.0×10^{-3}	3.7	29.8×10^{-3}	5.3	14
56-2c	16.7×10^{-3}	3.1	25.3×10^{-3}	4.7	15
56-2d	20.2×10^{-3}	3.6	29.2×10^{-3}	5.2	14
56-2f	22.0×10^{-3}	3.8	30.3×10^{-3}	5.2	14
56-3d	19.4×10^{-3}	3.4	28.1×10^{-3}	4.9	14
56-4a	20.7×10^{-3}	3.8	29.2×10^{-3}	5.3	14
56-4c	20.0×10^{-3}	3.5	28.7×10^{-3}	5.0	14

TABLE V

PERCENTAGE DEGRADATION OF I_{sc} AND EFFICIENCY IN TUNGSTEN AND SUNLIGHT

Cell Number	Tungsten I_{sc} Degradation (%)	Tungsten Efficiency Degradation (%)	Tungsten V_{oc} Degradation (%)	Sunlight I_{sc} Degradation (%)	Sunlight Efficiency Degradation (%)
56-1a	36	47	15	24	34
56-1d	28	41	15	18	32
56-1f	32	42	14	23	34
56-2a	46	57	16	33	47
56-2b	37	50	18	24	38
56-2c	48	59	19	34	47
56-2d	38	49	18	24	35
56-2f	34	46	15	23	37
56-3d	39	49	17	24	37
56-4a	40	51	17	26	41
56-4c	37	50	17	23	39

5. DISCUSSION OF RESULTS

The lack of any systematic relation between the various parameters of the cells altered by irradiation indicates that perhaps the mechanism of V_{OC} degradation is a random process varying with each individual cell, or that yet another parameter exists which has not been measured on which V_{OC} is dependent.

However, one striking fact is evident concerning the A factor, that is, that although the shape of the A factor versus V_{OC} curve is essentially similar before and after irradiation, the values of the A factor on all the cells measured decreased. Since the drift field cells used in these experiments are of a highly experimental nature, it is suggested future work on radiation damage to solar cells include an evaluation of I_o and A factor changes.

Also, the data presented includes only the results on the 10 ohm-cm base cells. The results of irradiation on the 25 ohm-cm cells were not available at the time of writing of this report.

REFERENCES

1. Final Report, "Development of an Improved Radiation Resistant Solar Cell," work performed by Electro-Optical Systems for NASA, Contract No. NAS5-3560

2. K. B. Wolfstirn, "Hole and Electron Mobilities in Doped Silicon from Radiochemical and Conductivity Measurements," J. Phys. Chem. Solids, Vol. 16, 1960, pp. 279-284

3. J. C. Irwin, "Resistivity of Bulk Silicon and of Diffused Layers in Silicon," Bell Telephone Systems Monograph No. 4092

APPENDIX

SOLAR CELL CONTINUITY EQUATION FOR DRIFT FIELD CELLS

(with a high field at the back of the cell)

ELECTRO-OPTICAL SYSTEMS, INC.
300 N. HALSTEAD ST., PASADENA, CALIFORNIA, 91107 • AREA CODE 213 681-4671, 449-1230 • TWX 213-577-0060
A Subsidiary of Xerox Corporation

26 July 1965

Dr. P. H. Fang
National Aeronautics and Space Administration
Goddard Space Flight Center
Greenbelt, Maryland

Dear Dr. Fang:

Enclosed is the data necessary to solve the solar cell continuity equation for drift field cells, with a high field at the back of the cell. The previous solution considered a high field at the front of the cell.

The equation governing the active or drift-field region of the cell:

$$D\frac{d^2n}{dx^2} + \left[\frac{dD}{dx} + \mu E\right]\frac{dn}{dx} + \left[E\frac{d\mu}{dx} + \mu\frac{dE}{dx} - \frac{1}{\tau}\right]n =$$

$$-\int_0^{\lambda} G\,N(\lambda)\,\alpha(\lambda)e^{-\alpha(\lambda)x}\,d\lambda \qquad (1)$$

becomes:

$$\frac{kT}{q}(C + Px)\frac{d^2n}{dx^2} + \left[P\left(\frac{KT}{q}\right) + \frac{.6x}{w^2}(C + Px)\right]\frac{dn}{dx} +$$

$$\left[P\frac{.6x}{w^2} + \frac{.6}{w^2}(C + Px) - \frac{1}{\tau}\right]n =$$

$$-\sum_{j=1}^{10} N(\lambda)_j\,\alpha(\lambda)_j\,e^{-\alpha(\lambda)_j x}\,(0.33R_j) \qquad (2)$$

upon substitution of the following identities again assuming a linear change in x of the variables:

$\mu = C + Px$, mobility of electrons in $cm^2\ sec^{-1}\ volt^{-1}$

$\frac{d\mu}{dx} = P$ in $cm\ sec^{-1}\ volt^{-1}$

$D = \mu(\frac{kT}{q}) = (C_1 + Px)\frac{kT}{q}$, diffusion constant of electrons by Einstein in relation in $cm^2\ sec^{-1}$

$\frac{dD}{dx} = P(\frac{kT}{q})$ in $cm\ sec^{-1}$

τ = electron minority carrier lifetime in secs

$E = \frac{0.6x}{w^2}$ = field in volts cm^{-1} where w is the boundary between the active (drift field) and passive regions

$\frac{dE}{dx} = \frac{0.6}{w^2}$ in volts cm^{-2}

The equation governing the passive layer toward the back of the cell is

$$\frac{d^2n}{dx^2} - \frac{n}{D\tau} = 0 \qquad (3)$$

assuming μ to be constant, E to be zero and the forcing term

$$-\int_0^{\lambda_G} N(\lambda)\alpha(\lambda)e^{-\alpha(\lambda)x}\,d\lambda$$

to be negligible. The solution is

$$n(x) = Ae^{-x/L} + Be^{x/L} \text{ where } L^2 = D\tau \qquad (4)$$

where $B = 0$ since $n \to 0$ as $x \to \infty$.

For evaluation of the constants A_1 and B_1 in any solution of Eq. 1, we can again describe the general solution of Eq. 1 as:

$$n_1(x) = A_1f_1(x) + B_1f_2(x) + f_3(x) \qquad (5)$$

and the solution of Eq. 3 as

$$n_2(x) = A_2 f_4(x) \tag{6}$$

The three boundary conditions necessary are defined by:

1. Considering the junction a sink for carriers:

$$n(x_j) = 0 \tag{7}$$

so that

$$n_1(x_j) = A_1 f_1(x_j) + B_1 f_2(x_j) + f_3(x_j) = 0 \tag{8}$$

2. Preserving continuity of carriers at $x = w$:

$$n_1(w) = n_2(w) \tag{9}$$

3. Preserving continuity of carrier flow at $x = w$:

$$D \frac{dn_1(w)}{dx} + E(w)\mu(w)\, n_1(w) = D \frac{dn_2(w)}{dx} \tag{10}$$

The second term in the left member comes about because of the discontinuity of the field strength at $x = w$. The carriers in the immediate vicinity of $x = w$ in the field region (region 1) are affected not only by diffusion, but also by the strong field.

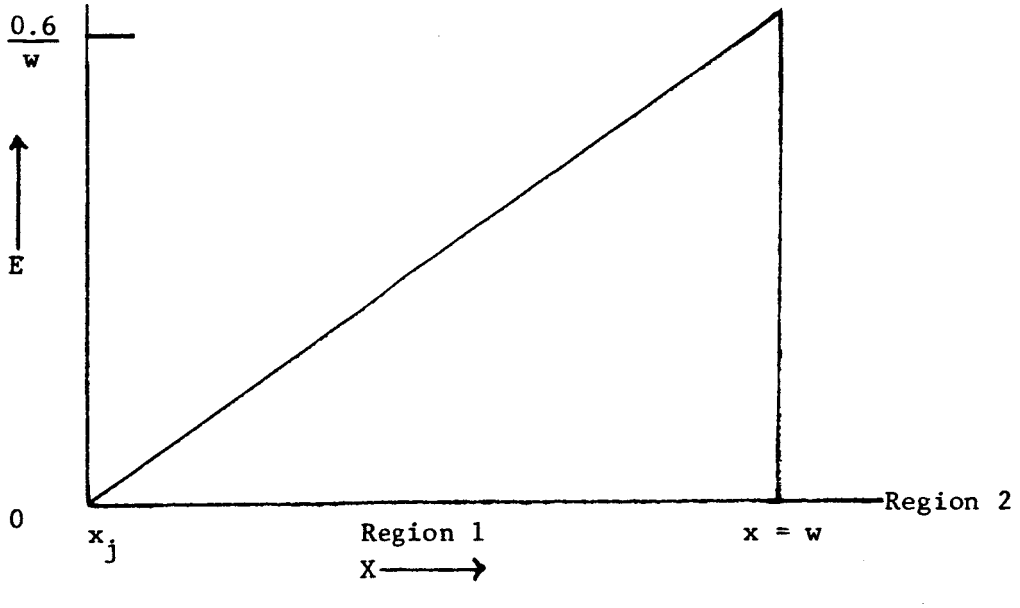

Substituting Eqs. 5 and 6 into Eq. 9:

$$A_1 f_1(w) + B_1 f_2(w) + f_3(w) = A_2 f_4(w) \tag{11}$$

and the derivatives of Eqs. 5 and 6 into Eq. 10:

$$A_1 f_1'(w) + B_1 f_2'(w) + f_3'(w) + \frac{E(w)\mu(w)\, n_1(w)}{D} = A_2 f_4'(w) \tag{12}$$

and by solving out of A_2 and rearrangement of terms we obtain:

$$A_1 \left[\frac{f_1'(w)}{f_4'(w)} - \frac{f_1(w)}{f_4(w)}\right]_1 + B_1 \left[\frac{f_2'(w)}{f_4'(w)} - \frac{f_2(w)}{f_4(w)}\right]_2 = \left[\frac{f_3(w)}{f_4(w)} - \frac{f_3'(w) + \dfrac{E(w)\mu(w)n_1(w)}{D}}{f_4'(w)}\right]_3 \tag{13}$$

This plus a rearranged form of Eq. 8:

$$A_1 f_1(x_j) + B_1 f_2(x_j) = -f_3(x_j) \tag{14}$$

are two linear equations of two unknowns which again can be solved by determinants yielding:

$$A_1 = \frac{\begin{vmatrix} [\,]_3 & [\,]_2 \\ -f_3(x_j) & f_2(x_j) \end{vmatrix}}{\begin{vmatrix} [\,]_1 & [\,]_2 \\ f_1(x_j) & f_2\, x_j \end{vmatrix}} \quad \text{and} \quad B_1 = \frac{\begin{vmatrix} [\,]_1 & [\,]_3 \\ f_1(x_j) & -f_3(x_j) \end{vmatrix}}{\begin{vmatrix} [\,]_1 & [\,]_2 \\ f_1(x_j) & f_2(x_j) \end{vmatrix}} \tag{15}$$

The numbered brackets corresponding to the numbered brackets in Eq. 13.

For purposes of programming, it should be noted that the only differences that exist between this solution and the previous solution are the altered expressions for E and dE/dx in the linearized form of the continuity equation and the altered form of the bracket 3 term in the determinant solution for A_1 and B_1.

Although the numerical values are the same as in the previous work, I reiterate them here for completeness:

1. For the Gaussian quadrature evaluation of the forcing integral:

	λ (in μ)	0.33R (in μ)	α (in cm^{-1})	N (in $cm^{-2}\ \mu^{-1}\ sec^{-1}$)
1.	0.429	2.20×10^{-2}	3.7×10^{4}	3.9×10^{17}
2.	0.465	4.92×10^{-2}	2.0×10^{4}	5.0×10^{17}
3.	0.526	7.23×10^{-2}	9.0×10^{3}	5.2×10^{17}
4.	0.607	8.88×10^{-2}	4.3×10^{3}	5.4×10^{17}
5.	0.701	9.77×10^{-2}	2.2×10^{3}	5.0×10^{17}
6.	0.799	9.77×10^{-2}	1.03×10^{3}	4.5×10^{17}
7.	0.893	8.88×10^{-2}	4.5×10^{2}	4.1×10^{17}
8.	0.974	7.23×10^{-2}	1.56×10^{2}	3.7×10^{17}
9.	1.035	4.92×10^{-2}	42.0	3.5×10^{17}
10.	1.071	2.20×10^{-2}	17.0	3.5×10^{17}

2. For the constants at $300^{o}K$:

$$\frac{kT}{q} = 0.026,\ \frac{q}{kT} = 38.5,\ C_1 = 1500\ cm^2\ sec^{-1}\ volt^{-1}$$

3. For the variables:

25μ wide drift field

$w = 2.5 \times 10^{-3}$ cm

$P = -5.8 \times 10^{5}$ cm sec^{-1}

$\tau = 10^{-5}$ secs
$= 3 \times 10^{-6}$ secs
$= 10^{-6}$ secs
$= 3 \times 10^{-7}$ secs
} at $x = x_j = 5 \times 10^{-5}$ cm

$\tau = 10^{-6}$ secs
$= 3 \times 10^{-7}$ secs
$= 10^{-7}$ secs
$= 3 \times 10^{-8}$ secs
} at $x = w = 2.5 \times 10^{-3}$ cm

50μ wide drift field

$w = 5 \times 10^{-3}$ cm

$P = -2.9 \times 10^{5}$ cm sec^{-1}

$\tau = 10^{-5}$ secs
$= 3 \times 10^{-6}$ secs
$= 10^{-6}$ secs
$= 3 \times 10^{-7}$ secs
} at $x = x_j = 5 \times 10^{-5}$ cm

$\tau = 10^{-6}$ secs
$= 3 \times 10^{-7}$ secs
$= 10^{-7}$ secs
$= 3 \times 10^{-8}$ secs
} at $x = w = 5 \times 10^{-3}$ cm

60μ wide drift field

$w = 6 \times 10^{-3}$ cm

$P = -2.4 \times 10^{5}$ cm sec^{-1}

$\tau = 10^{-5}$ secs
$= 3 \times 10^{-6}$ secs
$= 10^{-6}$ secs
$= 3 \times 10^{-7}$ secs
} at $x = x_j = 5 \times 10^{-5}$ cm

$\tau = 10^{-6}$ secs
$= 3 \times 10^{-7}$ secs
$= 10^{-7}$ secs
$= 3 \times 10^{-8}$ secs
} at $x = w = 6 \times 10^{-3}$ cm

80μ wide drift field

$w = 8 \times 10^{-3}$ cm

$P = -1.8 \times 10^{5}$ cm sec^{-1}

$\tau = 10^{-5}$ secs
$= 3 \times 10^{-6}$ secs
$= 10^{-6}$ secs
$= 3 \times 10^{-7}$ secs
} at $x = x_j = 5 \times 10^{-5}$ cm

$\tau = 10^{-6}$ secs
$= 3 \times 10^{-7}$ secs
$= 10^{-7}$ secs
$= 3 \times 10^{-8}$ secs
} at $x = w = 8 \times 10^{-3}$ cm

100μ wide drift field

$w = 10^{-2}$ cm

$P = -1.45 \times 10^{5}$ cm sec^{-1}

$\tau = 10^{-5}$ secs
$= 3 \times 10^{-6}$ secs
$= 10^{-6}$ secs
$= 3 \times 10^{-7}$ secs
} at $x = x_j = 5 \times 10^{-5}$ cm

$\tau = 10^{-6}$ secs
$= 3 \times 10^{-7}$ secs
$= 10^{-7}$ secs
$= 3 \times 10^{-8}$ secs
} at $x = w = 10^{-2}$ cm

125μ wide drift field

$w = 1.25 \times 10^{-2}$

$P = -1.16 \times 10^{5}$ cm sec^{-1}

$\tau = 10^{-5}$ secs
$= 3 \times 10^{-6}$ secs
$= 10^{-6}$ secs
$= 3 \times 10^{-7}$ secs
} at $x = x_j = 5 \times 10^{-5}$ cm

$\tau = 10^{-6}$ secs
$= 3 \times 10^{-7}$ secs
$= 10^{-7}$ secs
$= 3 \times 10^{-8}$ secs
} at $x = w = 1.25 \times 10^{-2}$ cm

150μ wide drift field

$w = 1.5 \times 10^{-2}$ cm

$P = -9.7 \times 10^{4}$ cm sec^{-1}

$\tau = 10^{-5}$ secs
$= 3 \times 10^{-6}$ secs
$= 10^{-6}$ secs
$= 3 \times 10^{-7}$ secs
} at $x = x_j = 5 \times 10^{-5}$ cm

$\tau = 10^{-6}$ secs
$= 3 \times 10^{-7}$ secs
$= 10^{-7}$ secs
$= 3 \times 10^{-8}$ secs
} at $x = w = 1.5 \times 10^{-2}$ cm

200μ wide drift field

$w = 2 \times 10^{-2}$ cm

$P = -7.25 \times 10^{4}$ cm sec^{-1}

$\left.\begin{array}{l} \tau = 10^{-5} \text{ secs} \\ = 3 \times 10^{-6} \text{ secs} \\ = 10^{-6} \text{ secs} \\ = 3 \times 10^{-7} \text{ secs} \end{array}\right\}$ at $x = x_j = 5 \times 10^{-5}$ cm $\left.\begin{array}{l} \tau = 10^{-6} \text{ secs} \\ = 3 \times 10^{-7} \text{ secs} \\ = 10^{-7} \text{ secs} \\ = 3 \times 10^{-8} \text{ secs} \end{array}\right\}$ at $x = w = 2 \times 10^{-2}$ cm

Please have the computer print out the identical information to that received from the previous solution. This will afford a direct basis of comparison between the two types of cells, high field in front and high field in back.

We are also at present preparing other data which includes different lifetime, mobility and field distribution and this will be submitted as soon as it is compiled. However, it would be interesting to note the results of the present solution before anything further is finalized.

Either Steve or I hope to see you at the Photovoltaic Specialists Conference there at Goddard in October.

Sincerely,

ELECTRO-OPTICAL SYSTEMS, INC.

G. P. Rolik, Engineer
Aerospace Electronics Division

GPR:slt